stellarator news

Published by Fusion Energy Division, Oak Ridge National Laboratory
Building 5700 P.O. Box 2008 Oak Ridge, TN 37831-6169, USA

Editor: James A. Rome Issue 125 April 2010
E-Mail: jar@ornl.gov Phone (865) 482-5643
On the Web at *http://www.ornl.gov/sci/fed/stelnews*

Wendelstein 7-X update

First module in final position

The first of five modules of Wendelstein 7-X (W7-X) is now in its final position. Two half-shells form the outer vessel around the magnet system, which eventually will be completely covered by the cryostat. For assembly of the W7-X cryostat this step is important and spectacular at the same time: First, the ~100 ton magnet module is lifted into the lower part of the cryostat vessel and positioned with millimeter accuracy. Then the top half closes the cryostat. Equipped with super-insulation, the outer vessel forms a huge "refrigerator." Inside, the magnetic field coils are operated close to absolute zero. Hence, the superconductors can provide — almost without losses — the specially optimized magnetic field cage of W7-X.

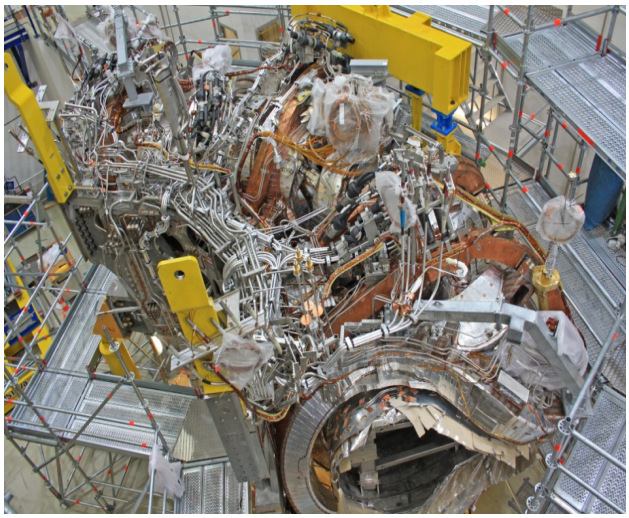

Fig. 1. Magnet module before transfer into the lower shell of the outer vessel.

The effort is necessary to fulfill the mission of the experiment: to demonstrate the feasibility of steady-state operation of an optimized stellarator reactor.

This technically challenging assembly step was anticipated with great suspense, because the procedure was bearing some (literally) heavy potential problems.

In this issue . . .

Huge masses must be exactly maneuvered into position, with an accuracy that is dictated by stellarator physics. Then the upper part of the cryostat vessel is installed. Less obvious are hundreds of work-weeks of preparation: In addition to the assembly, detailed computer models had to be developed. Again and again the positions of the components were measured; data were analyzed and then added to the geometrical data bank. Increasingly accurate models were developed showing with very high accuracy how the individual parts of Wendelstein 7-X had been manufactured. Only at this stage was it possible to verify whether collisions would occur. Hundreds of meters of pipes and insulation sheets must not touch or damage coils, supply lines, or other parts of the device. Without modern, computer-aided procedures the assembly of these components would not have been possible, since the movement of the parts during cooling and with magnetic field applied had to be taken into account.

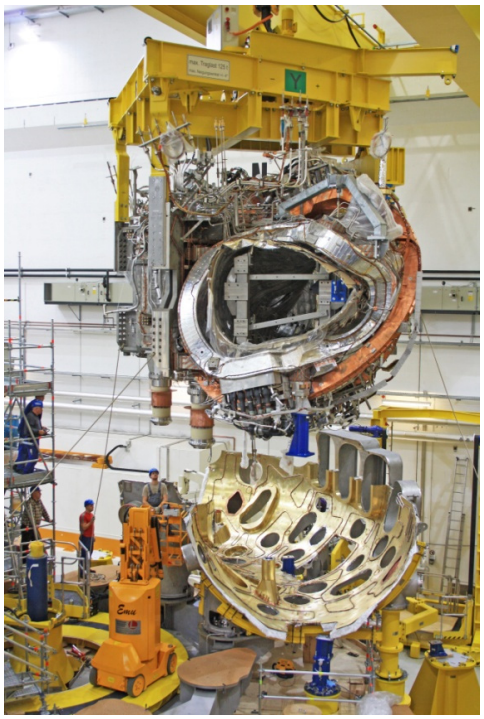

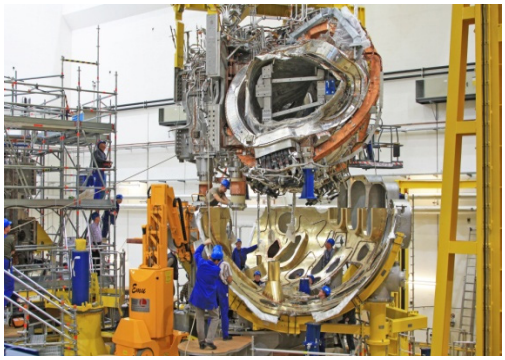

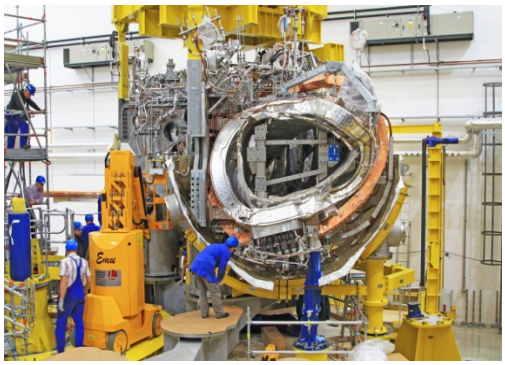

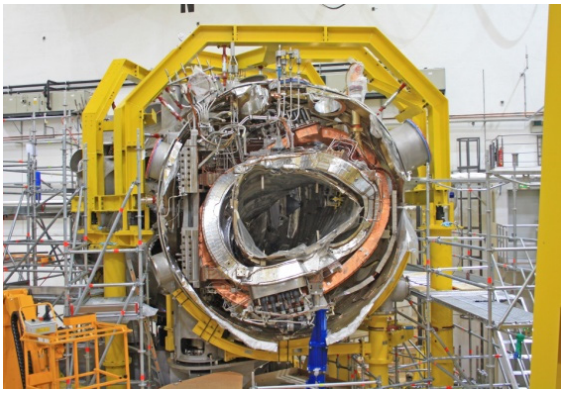

Fig. 2. Moving the magnet module into place onto the lower part of the cryostat.

However, one cannot rely on computer models alone: Dimensions and alignments had to be checked repeatedly. In fact, a few errors were found and corrected. Insertion of the magnet module could not start before all critical positions were verified. Finally, the eyes of 12 humans had to carefully observe the lowering procedure so that in case of doubt the process could be interrupted.

Once the heavy load reached its final position, the reward was the closing of the cryostat vessel as predicted. Now, the next step is the installation of the ports. For each module about 50 large, specially designed tubes provide access

to the plasma vessel for pumping, heating and cooling, and observing the plasma.

The cryostat

The cryostat is a chamber that contains the superconducting coils. The plasma vessel, weighing 35 tons, and the two shells of the outer vessel form the casing of the cryostat. This casing is perforated by numerous ports to allow access to the interior of the plasma vessel. The inner wall of the cryostat is covered with insulation and layered panels that form the so-called cryoshield, which is cooled to –203°C (70 K) during operation. A vacuum is maintained within the cryostat, thereby nearly eliminating the heat conduction. Together with the cryoplant, Greifswald's largest "refrigerator" can keep a mass of 425 tons at 4 K. In order to provide the necessary cooling power of about 7 kW at 4.5 K, 1640 kW of electrical input power for the compressor and other components is required.

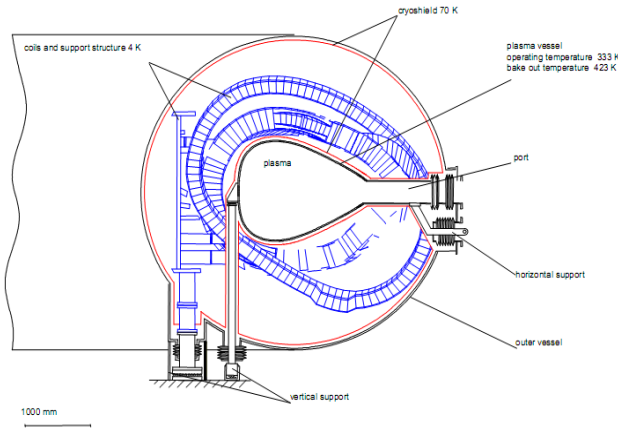

Fig. 3. The cryostat, which encompasses the magnet system, is one of the central parts of the W7-X infrastructure.

R. Wolf, A. Dinklage, B. Kemnitz
IPP Greifswald
Greifswald, Germany

Experimental study on non-local transport phenomenon in LHD

Because burning plasmas are considered to be highly autonomous, the number of "knobs" that may be used to control such plasmas is limited. Nevertheless, even in burning plasmas, dissipative structures in the turbulent transport such as internal transport barriers and H-mode pedestals should be established. Recently, the significance of nonlocality (i.e., an interaction between two distant points) in heat transport has become prominent in studies of magnetically confined plasmas [1, 2]. External control of the formation of dissipative structures in burning plasmas requires a clear understanding of the nonlocality of heat transport and its dynamics. A nonlocal heat transport phenomenon (e.g., a rapid rise in core electron temperature T_e in response to edge cooling) is the most prominent example of nonlocality in heat transport, observed in many tokamaks (e.g., Ref. [3]) and recently in a helical system [4, 5]. Here a brief summary of the nonlocal transport phenomenon observed in the Large Helical Device (LHD) and results of a new analysis of the phenomenon are presented.

An experiment elucidating the nonlocal transport phenomenon has been carried out in high-temperature, low-density LHD plasmas. Hydrogen is used as the working gas. The plasma is usually heated by a tangential negative-ion-based neutral beam injection (nNBI) system and/or an electron cyclotron heating (ECH) system. A large fraction (~70%) of the negative-ion-based neutral beam power goes into the electrons due to the high acceleration energy (~140–180 keV). Thus the ratio of electron temperature to ion temperature, T_e/T_i is usually greater than unity in the experiment, and the electron loss channel dominates the ion loss channel. In order to track the temporal behavior of T_e with a high time resolution ($\delta t \sim 1$ s), the electron cyclotron emission (ECE) is measured from the inboard side of LHD with a 32-channel heterodyne radiometer. The typical spatial resolution of the heterodyne radiometer is about 1 cm at the position of the half plasma minor radius [6]. The heterodyne radiometer measurement of T_e is in good agreement with that from the YAG Thomson scattering system [7]. A 13-channel far-infrared (FIR) interferometer [8] is used to measure the temporal behavior of the electron density n_e, and the n_e profile is reconstructed by using the Abel inversion technique based on the data measured. In order to cool the edge region of the LHD plasma, a tracer-encapsulated solid pellet (TESPEL) [9] is injected into the LHD plasma usually from the outboard side of LHD.

The TESPEL consists of polystyrene [$CH(C_6H_5)CH_2$] [10] as an outer shell, the diameter of which ranges from

around 400 μm to 900 μm, and tracer particles as an inner core. In the nonlocal transport phenomenon experiment, no tracer impurity is loaded into the TESPEL to reduce the possibility of improving the heating efficiency by the nNBI attributed to the increased effective ionic charge. The TESPEL penetrating into the LHD plasma ablates typically within ~1 ms [11] and provides a small amount of cold ions and electrons. These decrease T_e at the periphery of the LHD plasma, and this negative temperature perturbation propagates toward the core with a certain delay (cold pulse propagation).

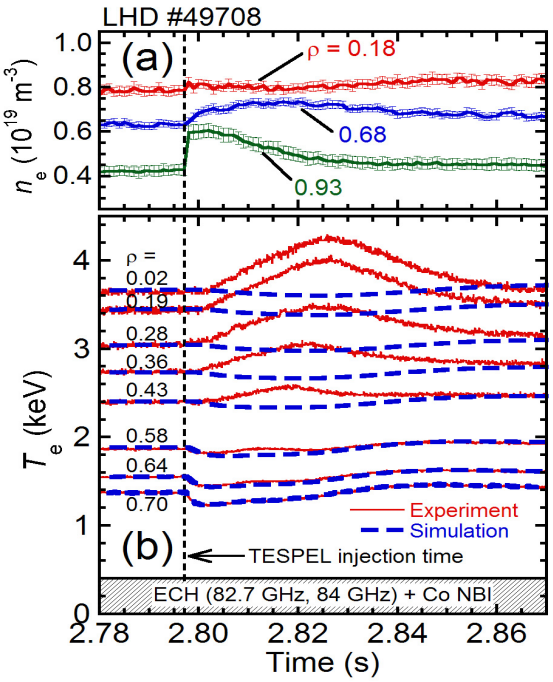

Fig. 1. Temporal evolution of (a) electron density measured with the FIR interferometer at three different normalized minor radii and (b) electron temperature (solid lines) measured with the ECE radiometer at different normalized minor radii. In (b) the simulated electron temperature (broken lines) is also plotted. The TESPEL injection time is indicated as the vertical dashed line.

Figure 1 shows typical temporal behavior of n_e and T_e before and after the onset of the nonlocal transport phenomenon induced by TESPEL injection in LHD. For this discharge, the major radius at the magnetic axis R_{ax} is 3.5 m, the average minor radius a is 0.58 m, and the magnetic field on axis B_{ax} is 2.829 T. Within the time displayed in Fig. 1, the plasma is heated continuously by nNBI in the co-direction (injected power ~2 MW) and ECH with 82.7-GHz and 84-GHz gyrotrons to achieve fundamental resonance heating (total injected power ~ 1 MW). The ECH power is absorbed inside ρ ~ 0.2. As can be easily seen in Fig. 1(b), the core T_e rises sharply in response to the edge cooling associated with TESPEL injection. In this case, the peak of the incremental T_e in response to the edge cooling seems to propagate toward the center of the plasma on a time scale of the diffusive nature, and it becomes higher toward the center of the plasma. as T_e rises in the core region, neither density peaking [see Fig. 1(a)] nor significant change in low-m magnetohydrodynamics (MHD) modes is observed. In order to estimate how far the T_e measured deviates from that based on a simple diffusion model, the perturbation equation,

$$\frac{3}{2}n_e(r)\left[\frac{\partial}{\partial t}\delta T_e(r,t)\right] = \nabla\cdot[n_e(r)\chi_e^{PB}(r)\nabla\delta T_e(r,t)]$$

is solved numerically by using the time-dependent boundary condition. Here, δT_e is the electron temperature perturbation and χ_e^{PB} is the electron thermal diffusivity estimated by the power balance analysis. In the simulation, the electron density perturbation is ignored and slab and cylindrical geometry are used for simplicity. As shown in Fig. 1(b), the temporal behavior of T_e in the outer region of the plasma (ρ > 0.6) agrees well with that predicted by the simple diffusion model. However, the discrepancy between measured and simulated T_e is quite significant in the core (ρ < 0.6), where it is far from the TESPEL penetration region (ρ > ~ 0.9).

The nonlocal transport phenomenon in LHD has some characteristics in common with tokamaks; the nonlocal T_e rise in LHD takes place in a high-temperature, low-density regime, it has been observed not only after the TESPEL injection but also after injection of a small solid hydrogen pellet [12] and a controlled gas puff (even when argon is used) [13].

Meanwhile, various new aspects of the nonlocal transport phenomenon have been revealed by the LHD experiments. For example, a nonlocal T_e rise in response to edge cooling is observed in various plasmas; a nonlocal T_e rise is also observed in plasmas heated only with ECH (i.e., in a net-current-free plasma), which completely rules out toroidal plasma current and high-energy ions as causes for the nonlocal T_e rise. And even a purely nNBI-heated plasma shows a nonlocal T_e rise, indicating that high-energy electrons cannot be the cause. Another feature of the nonlocal transport phenomenon in LHD is that the response time of the core T_e to the edge cooling increases both with increasing collisionality in the core plasma and with electron temperature gradient scale length in the outer region [12]. The appreciable delay in the core T_e rise after the edge cooling is also observed in many tokamaks (e.g., [14]). However, it is not observed with an increase in n_e in the RTP [14]. In particular, even when the emergence of the nonlocal T_e rise is delayed, the start time of the T_e rise in the core (ρ < 0.4) remains uniform in space.

It is important to investigate the properties of turbulence in plasmas that exhibit nonlocal transport phenomenon. The properties of density fluctuations have usually been measured as an indicator of plasma turbulence. Since the amplitude of turbulent density fluctuations can be modulated by long-range turbulent structure (e.g., zonal flow) through the parametric modulational instability [15], an envelope of the turbulent density fluctuation would provide information about the spatial structures of the long-range turbulence. The envelope of density fluctuations measured with reflectometry is modulated with a low frequency (≤2 kHz), which clearly suggests the existence of a long-range turbulent structure in the plasma where the non-local transport phenomenon appears [16]. Recent analysis of ECE signals also finds a macroscale ($0.2 \le \rho \le 0.7$) turbulent structure in plasmas with the nonlocal transport phenomenon [17].

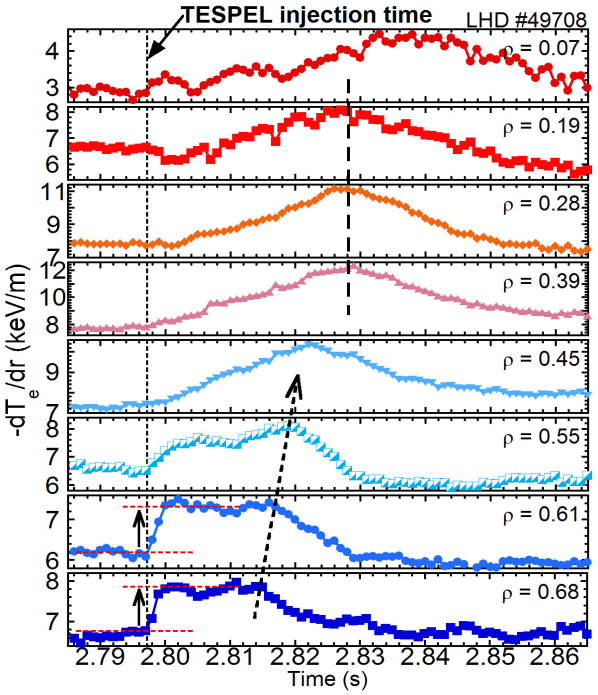

Fig. 2. Temporal evolution of the measured electron temperature gradient at different normalized minor radii. All data are plotted at 1 ms intervals. TESPEL injection time is indicated by the vertical short-dashed line.

Here we review a new analysis result for the nonlocal transport phenomenon. Figure 2 shows the temporal evolution of the measured T_e gradient $-dT_e/dr$ before and after the onset of the nonlocal transport phenomenon. Immediately after the edge cooling initiated by the TESPEL injection, dT_e/dr increases sharply in the region extending from $\rho \sim 0.6$ to at least $\rho \sim 0.7$, as seen in Fig. 2. Although this dT_e/dr jump is likely affected by the increase in n_e due to the TESPEL injection, the increased dT_e/dr is sustained for a while, unlike the usual case. Thus, a first-order transition of electron heat transport, which is categorized by a discontinuity in dT_e/dr [18], appears over a wide region (at least 6 cm wide) in the periphery of the plasma.

At about the same time, a second-order transition in the electron heat transport, which is characterized by a discontinuity in $d(dT_e/dr)/dt$ [18], appears over a wide region ($0.28 < \rho \le 0.45$, about 10 cm wide) in the plasma core. These indicate the existence of large-scale coherent structures in both core and edge regions, which are on a scale larger than a typical microturbulent eddy size (a few millimeters in this case), and their interaction can cause the nonlocal T_e rise. The macroscale turbulent structure observed in the reflectometer and ECE signals could support the linkage of the large-scale coherent structures.

As shown in Fig. 3, the flux-gradient relation just after the edge cooling shows the jumps in core heat flux and edge dT_e/dr. This suggests that the core turbulence is suppressed through interaction with the edge turbulence, not due to the expansion of the mechanism of edge heat transport improvement. Afterward the second-order transition of the electron heat transport as a backward transition appears spontaneously outside the core ($\rho > 0.45$) and seems to propagate towards the core (indicated by the short-dashed arrow in Fig. 2). This suggests that the large-scale coherent structure in the edge region no longer exists at this phase. It should be noted, however, that in the core region ($0.19 \le \rho \le 0.39$), the backward second-order transition of the electron heat transport seems to start simultaneously (indicated by the long-dashed line in Fig. 2). This indicates that the core large-scale coherent structure still exists at this time. Consequently, the core T_e rise due to the nonlocal transport phenomenon does not appear to require the well-known turbulent transport reduction process, the breaking of turbulent eddies [19] (i.e., the disappearance of the nonlocality) in the core region.

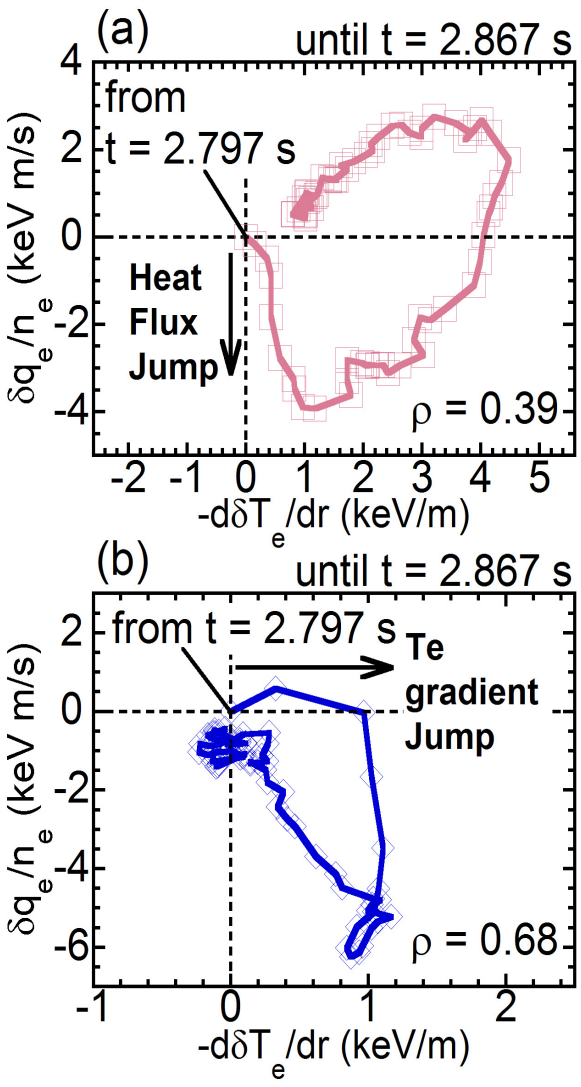

Fig. 3. Relationship between the perturbed normalized electron heat flux and the perturbed electron temperature gradient at (a) ρ = 0.39 and (b) ρ = 0.68. All data are plotted at 1 ms intervals.

This result provides new insight into nonlocal transport phenomena; the nonlocal transport phenomenon in LHD takes place as a result of the linkage of large-scale coherent structures in both core and edge regions. The detailed mechanism for the formation of these structures and its linkage remains an open question. Further work on this challenging issue will be discussed in a future paper.

Acknowledgements

The author acknowledges all of the technical staff of the National Institute for Fusion Science (NIFS) for their excellent support. I also would like to thank Emeritus Prof. O. Motojima (former Director of NIFS) and Prof. A. Komori (current Director of NIFS) for their continuous encouragement. This work is partly supported by a Grant-in-Aid for Scientific Research (B) (No. 19340179) from the Japan Society for the Promotion of Science, a Grant-in-Aid for Young Scientists (B) (No. 19740349) from MEXT Japan and a NIFS budgetary Grant-in-Aid No. NIFS09ULHH510.

Naoki Tamura
High Temperature Plasma Physics Research Division
National Institute for Fusion Science
322-6 Oroshi-cho Toki, Gifu, 509-5292 JAPAN
E-mail: tamura.naoki@LHD.nifs.ac.jp

References

[1] K. Ida et al., Phys. Rev. Lett. **101** (2008) 055003.

[2] S. Tokunaga et al., Nucl. Fusion **49** (2009) 075023.

[3] K. W. Gentle et al., Phys. Rev. Lett., **74** (1995) 3620.

[4] N. Tamura et al., Phys. Plasmas **12** (2005) 110705.

[5] S. Inagaki et al., Plasma Phys. Control. Fusion, **48** (2006) A251.

[6] K. Kawahata et al., Rev. Sci. Instrum. **74** (2003) 1449.

[7] K. Narihara et al., Rev. Sci. Instrum. **72** (2001) 1122.

[8] K. Kawahata et al., Rev. Sci. Instrum. **70** (1999) 707.

[9] S. Sudo., J. Plasma Fusion Res. **69** (1993) 1349.

[10] K. Nagai et al., J. Polym. Sci. A: Polym. Chem. **38** (2000) 3412.

[11] N. Tamura et al., Rev. Sci. Instrum. **79** (2008) 10F541.

[12] N. Tamura et al., Nucl. Fusion **47** (2007) 449.

[13] N. Tamura et al., J. Phys.: Conf. Ser. **123** (2008) 0120023.

[14] P. Galli et al., Nucl. Fusion **39** (1999) 1355.

[15] P. H. Diamond et al., Plasma Phys. Control. Fusion **47** (2005) R35.

[16] S. Inagaki et al., Plasma Fus. Res. **3** (2008) S1006.

[17] S. Inagaki et al., in Proc. 22nd IAEA FEC (2008), IAEA-CN-165/EX/P5-10.

[18] K. Ida et al., J. Phys. Soc. Jpn. **77** (2008) 124501.

[19] H. Biglari et al., Phys. Fluids B **2** (1990) 1.

High-field pulsed Allure Ignition Stellarator

To raise interest in fusion energy, a new concept for a low-cost stellarator has been developed. The essence of the concept is a two-period stellarator located on a vertical plane to ease maintenance operations. A double-hull toroidal vessel arrangement allows the flow of a liquid Li compound that provides heat extraction and serves as a plasm-facing material or first wall (FW). The strategy is to aim for a small device working at high density and extremely high field. Stellarators are particularly suited for this strategy if the Sudo limit applies under the proposed conditions.

Ignition in a small device (not bigger than a car) seems feasible. Certain innovations and rules need to be followed to achieve low cost. High reaction rate, DD ignition-like pulses, and then DT ignition in the same small stellarator core can be performed in phases as interest rises.

Stimulation of nuclear fusion commercial technology requires generation of private industrial sector interest in fusion energy. Similar to a snowball effect, if a reasonably low investment translates into a high-reaction-rate device or ignition, then exponential growth of interest in fusion energy would likely occur. Seeking such a phenomenon should be pursued despite some risk of failure.

Summary of objectives, concept, and strategy

The main objective of the present development is to maximize the interest generated in the industrial and political communities for a given investment.

The Allure Ignition Stellarator (AIS) is a small, high-field, high-density, two period modular stellarator located on a vertical plane, which could be attractive to the industry because of its ease of maintenance, small size, simplicity, and resemblance to present nuclear fission reactors.

The essential points of the strategy to achieve the objective are as follows.

i) Lower the cost of the stellarator and the R&D process. This would be achieved by means of engineering innovation and minimization of negligible elements. Use of innovative construction methods, for example the additive manufacturing proposed in Ref. [1] or special toroidal milling machines [2], are just two of several possible methods to lower construction costs. To lower operational costs, the stellarator should be designed for a low pulse repetition rate, the order of a few pulses per month.

ii) Exploit the advantages of stellarators over tokamaks, focusing on the achievement of high plasma density in a small high-field device, along with steady and simple pulsed power supplies and avoidance of current drive systems.

iii) Execute in two phases to create and sustain interest:

- First: Use cryo-cooled pulsed (~ 0.1 s) copper coils for a ~3 m (or smaller) high stellarator. Operate initially with HH and DD fuel and later, after funds are raised, some DT ignition pulses.
- Second: Upgrade the system with YBCO superconducting coils to produce longer pulses.

Concept of the Allure Ignition Stellarator

The AIS is a small, high-field, two-period modular stellarator. The reactor vessel is located on a vertical plane to ease maintenance.

In this context, high field means the field necessary to achieve ignition once the reactor size is specified. Since low-cost ignition is a main objective, relatively small size devices are favored.

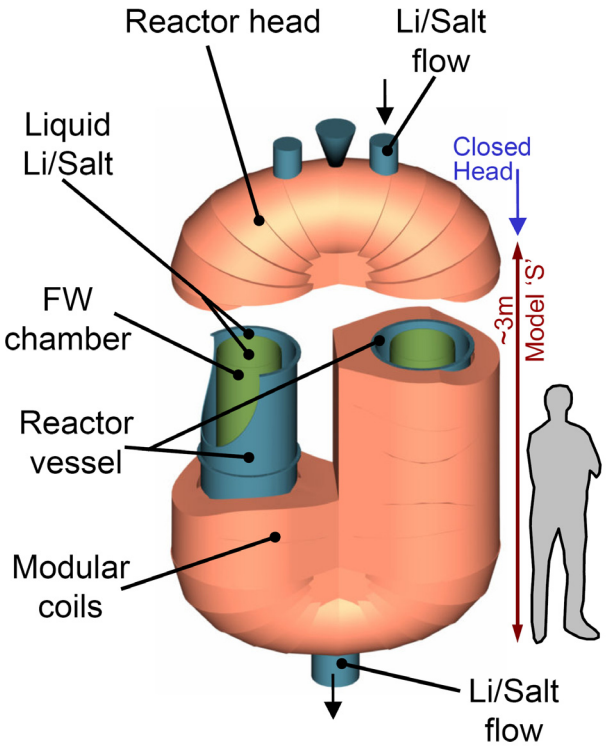

Fig. 1. Model S (Small) Allure Ignition Stellarator, working at B_0 ~ 35 T.

The stellarator is based on a double-hull toroidal vessel located in a vertical position and shaped somewhat like a twisted racetrack, as depicted in Figs.1 and 2.

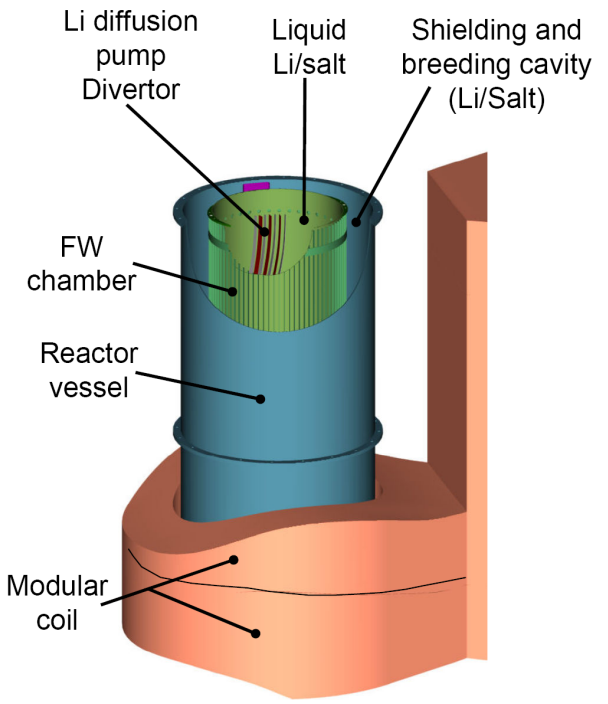

Fig. 2. Detail of the vessel, chamber, and divertors of AIS.

The vertical orientation of AIS is chosen to provide fast and simple maintenance by means of vertical handling. Few elements of simple shape are sought.

A double-hull structure defines a cavity filled with a liquid Li compound that flows from top to bottom. The inner hull corresponds with the FW chamber, and the outer hull is the reactor vessel. Both are divided into several segments to allow disassembling and FW chamber replacement.

A fraction of the Li compound may be allowed to enter the inner FW chamber through calibrated nozzles, to serve as a plasma wall-facing material. For the short-pulsed AIS the Li compound is avoidable. The liquid Li compound could be a mixture of liquid Li and LiD or Flibe with the correct proportion to achieve neutron shielding, as well as tritium breeding and cooling and to provide a low-Z facing component.

The divertors of the stellarator should preferably be innovative longitudinal lithium diffusion pumps.

Several sets of modular coils surround the reactor vessel. The coils and vessel are jointly designed to allow replacement if necessary. The coil casings interlock with maximum contact surface to form several monolithic sets that handle the Lorentz forces. The monolithic sets also interlock with maximum contact surfaces to handle the centering forces. The end result is a single block without a central toroidal hole. This structure is devised to handle strong magnetic forces. Openings for heating and diagnostics are likewise minimized.

The reactor head is composed of coil monolithic sets and the curved section of the double hull. It is arranged to be removed vertically for relatively fast access into the internals of the vessel.

A twin mirror configuration, somehow similar to a two-period Helias stellarator with diminished twist, is the most suited for the proposed geometry. Coil shapes, monolithic sets, and double-hull geometry are optimized together to obtain a balanced combination of sufficient plasma confinement properties and reactor maintainability, especially for the replacement of failed coils or a worn FW chamber. Fast maintenance is then possible due to the low number of elements and the vertical access.

Small, high-field stellarators

Since the objective is to have a small ignited device, it is necessary to determine the minimum size for ignition as a function of the magnetic field.

The Sudo limit [3, 4] relates the maximum plasma density achievable with a given heating power density P/V in a certain magnetic field B,

$$n < K_s\,(P/V)^{\nu}\,B^{\eta}. \qquad (1)$$

Fulfilment of power balance requires

$$dW/dt = P_{ext} + P_{\alpha} - P_{loss},$$

$$P_{loss} = W/\tau_E\,.$$

In steady state,

$$P_{ext} + P_{\alpha} = P_{loss}\,.$$

For ignition there is no external heating:

$$P_{ext} = 0,$$

so

$$P_{\alpha} = P_{loss} = P_{heating} = P,$$

resulting in

$$3\,k_B n T V/P_{\alpha} \;= \tau_E\,. \qquad (2)$$

The alpha power P_{α} relates to the reaction rate parameter $\langle\sigma v\rangle_{DT}$, density n, and fusion product alpha energy W_{α} as follows

$$P_{\alpha} = 1/4\;W_{\alpha}\,\langle\sigma v\rangle_{DT}\,n^2\,V = c\;T^{\phi}\,n^2\,V\,, \qquad (3)$$

where the reaction rate parameter is approximated by

$$\langle\sigma v\rangle_{DT} \propto T^{\phi}\,.$$

Considering the scaling law for the confinement time

$\tau_E = C_0 R^{\varphi} a^{\theta} B^{\alpha} n^{\delta} P^{-\sigma} \iota^{0.41}$,

$R = A\,a$ (A = aspect ratio),

$R^{\varphi} a^{\theta} = k_R(A, \varphi, \theta)\ V^{(\varphi+\theta)/3} = k_R V^{\epsilon}$,

and because $k' = C_0 k_R \iota^{0.41}$,

$$\tau_E = k'\, V^{\epsilon}\, B^{\alpha}\, n^{\delta}\, P^{-\sigma} \qquad (4)$$

because $\langle\beta\rangle \propto nT/B^2$. (5)

Here

P : heating power (MW)

T : average plasma temperature (keV), $T_i = T_e = T_{ave}$

V : plasma volume (m^3)

n : average plasma density (10^{20} m^{-3})

$B_0 = B$: magnetic field on axis (T)

From Eqs. (2) to (5) results

$$3\, k_B n T V / P = k'\, V^{\epsilon}\, B^{\alpha}\, n^{\delta}\, P^{-\sigma}. \qquad (6)$$

Combining (1), (3), (5), and (6) and keeping B and V, the minimum volume for ignition can be written as:

$$V_{ig} \approx k / B^{\lambda}. \qquad (7)$$

In particular for the density limit scaling of the W7-AS stellarator [4]

$$n_{W7\text{-}DL} = 1.46\,(P/V)^{0.48}\, B^{0.54}\ [10^{20}\ m^{-3}],$$

$$\langle\sigma v\rangle \approx 7.81 \times 10^{-26}\, T^{3.2} \quad \text{for } T \in [5,8] \text{ keV}.$$

The scaling law for confinement [4],

$$\tau_{E,ISS04} = 0.465\, R^{0.64}\, a^{2.28}\, B^{0.84}\, n^{0.54}\, P^{-0.61}\, \iota^{0.41}.$$

If we assume a beta limit $\langle\beta\rangle = 5\%$, an aspect ratio $A = 5.9$, and $\iota = 2/3$, then

$$V_{ig}\ (m^3) \approx 2.04 \times 10^6 / B^{4.13} \quad (B \text{ in T}). \qquad (8)$$

The expression in Eq. (8) is plotted in Fig. 3.

The parameter k in Eq. (7) strongly depends on the selected expressions for the Sudo limit and the τ_E scaling, but the parameter λ depends only weakly on these choices.

The volume required for stellarator ignition scales with the inverse of more than the fourth power of **B**, according to Eq. (8). This suggests that seeking high fields, particularly for the first phase (copper coils) Allure, should be considered a priority for stellarators. This approach has a certain resemblance to the FIRE and IGNITOR concepts for tokamaks. Nevertheless, this approach is crucial for stellarators as also suggested in Ref. [6].

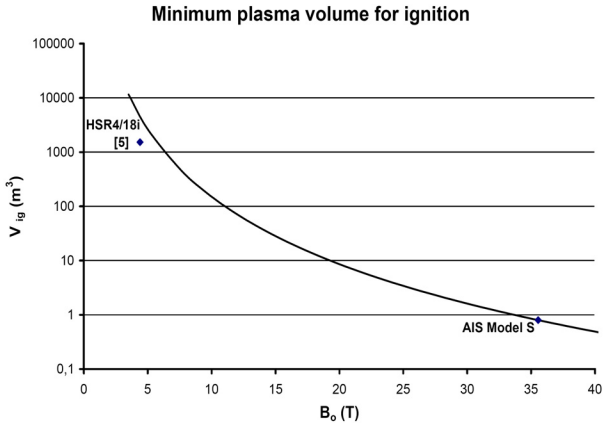

Fig. 3. Minimum plasma volume for ignition. Values for the HSR4/18i design [5] and one of the AIS models, the "Model S," are shown for comparison.

Future work and conclusion

Several major issues remain, in particular finding relatively low-cost means to generate about 200–300 MW of heating power for DD ignition-like pulses as well as the feasibility of relatively inexpensive power supplies for the coils and heating systems for pulses of the order of 0.1 s.

Plasma-wall interaction is a concern, but the problem should decrease for fast, powerful plasma core heating during short pulses.

The strategy proposed resembles somewhat to the philosophy followed in inertial confinement fusion, in particular the aim of low pulse repetition rate at high neutron rate and delaying the issue of plasma-wall interaction and net energy production for a subsequent development phase.

Devising heating methods and power supplies appropriate for the objective remain for a future work.

Vicente M. Queral, J.A. Romero, J.A. Ferreira
Laboratorio Nacional de Fusión,
CIEMAT*, Spain
E-mail: vicentemanuel.queral@ciemat.es
* The views expressed do not necessarily reflect those of CIEMAT.

References

[1] Lester M. Waganer et al., and ARIES Team, "ARIES-CS coil structure advanced fabrication approach," Fusion Sci. Technol. **54**. (2008) 655–672.

[2] Vicente Queral, "UST_1, a small, low-cost stellarator," *Stellarator News*, issue 118, December 2008.

[3] S. Sudo et al., "Scalings of energy confinement and density limit in stellarator heliotron devices," Nucl. Fusion **30** (1990) 11–21.

[4] A. Weller, et al., "International Stellarator/Heliotron Database progress on high-beta confinement and oper-

ational boundaries," Nucl. Fusion **49** (2009) 065016.

[5] Yu. Igitkhanov et al., "Status of HELIAS reactor studies," Fusion Eng. Des. **81** (2006) 2695–2702.

[6] Takuya Goto and Yuichi Ogawa, "Optimization of plasma performance for a helical fusion reactor," Fusion Eng. Des. **81** (2006) 1251–1255.

Horst Wobig retirement gift

This mural was presented to Horst Wobig by his colleagues on the occasion of his retirement.

Presumably this scene is on top of Mount Wendelstein.

7th Coordinated Working Group Meeting, IPP Greifswald, June 30–July 2, 2010

The 7th Coordinated Working Group Meeting to be held at IPP Greifswald from Wednesday, June 30 through Friday, July 2, 2010 (one week after the EPS meeting in Dublin).

The Coordinated Working Group Meeting (CWGM) implements and coordinates international collaborations in stellarator/heliotron research. The work is intended to contribute to the International Stellarator/Heliotron Confinement and Profile Database [ISH-C(P)DB]. The meeting is open to everybody in the magnetic confinement fusion community.

CWGMs have the character of a working meeting. The sessions are coordinated by a topic leader. The purpose of the sessions is to progress towards a well-specified working goal. The session leaders of this meeting will be announced in due course.

Proposals for sessions are welcome at any time; the realization of sessions, however, depends on the availability of time slots and its importance for joint collaborations.

CWGM and its related database activities have been conducted under the auspices of the IEA Implementing Agreement of Development of Stellarator-Heliotron Concepts.

A tentative list of topics is:

- Stellarator/heliotron H-mode survey
- High-beta, MHD physics
- Magnetic island/iota/shear
- Validation of transport models
- Edge turbulence database
- Impurity transport

If you are interested in attending the meeting, please register electronically at the meeting Web site by May 31, 2010: http://www.ipp.mpg.de/~dinklage/CWGM7

Andreas Dinklage and Robert Wolf
Local organizers